A fluorescent quenching performance enhancing principle for carbon nanodot-sensitized aqueous solar cells

Haimin Zhang[a,b], Yun Wang[b], Porun Liu[b], Yibing Li[b], Hua Gui Yang[b], Taicheng An[c], Po-Keung Wong[d], Dan Wang[b], Zhiyong Tang[b], and Huijun Zhao[a,b,*]

[a] Centre for Environmental and Energy Nanomaterials, Institute of Solid State Physics, Chinese Academy of Sciences, Hefei 230031 (China)

[b] Centre for Clean Environment and Energy, Gold Coast Campus, Griffith University, Queensland 4222 (Australia)

[c] State Key Laboratory of Organic Geochemistry, Guangzhou Institute of Geochemistry, Chinese Academy of Sciences, Guangzhou 510640 (China)

[d] School of Life Sciences, The Chinese University of Hong Kong, Shatin, NT, Hong Kong SAR (China)

Corresponding author: Fax: +61-7-55528067; Tel: +61-7-55528261; E-mail: h.zhao@griffith.edu.au

Abstract

We report a fluorescent quenching principle capable of markedly enhancing the conversion efficiency of carbon nanodots (CNDs)-sensitized aqueous solar cells (CNDs-ASCs). A conversion efficiency of 0.529%, over 4-times of the best conversion efficiency reported for CNDs-sensitized solar cells, is achieved with a cell constructed using CNDs as the sensitizer and aqueous I^-/I_3^- electrolyte serving a dual-function as the recombination blocker (fluorescent quencher) and redox mediator. The results confirm that the significantly enhanced utilization efficiency of the photo-excited electrons resulting from the efficiently quenched fluorescent emission of CNDs sensitizer by I^- is responsible for the markedly improved conversion efficiency of CNDs-ASCs. The findings of this work validate a principle that could be widely applicable for enhancing the performance of solar cells employing other fluorescent quantum dots/nanodots sensitizers.

Keywords: Fluorescent quenching; Aqueous solar cells; Carbon nanodot sensitizer; Iodide quencher; Natural biomass

Introduction

A variety of quantum dots (QDs) and nanodots (NDs) has been utilized as sensitizers for solar cells [1-6]. Although QDs/NDs-sensitized solar cells (QDs/NDs-SSCs) have many attractions, in general they possess lower conversion efficiency (<7%) when compare to dye-sensitized solar cells and newly reported perovskite-based solar cells [7-10]. It is well known that the majority of QDs/NDs are fluorophores [11-13]. When they are used as sensitizers in solar cells, the fluorescent emission is, in effect, a charge recombination pathway, leading to a dramatically reduced utilization efficiency of the photo-excited electrons for electricity generation, which is a major factor responsible for low conversion efficiencies of QDs/NDs-SSCs. On this basis, we hypothesize that the utilization efficiency of the photo-excited electrons generated by the fluorescent sensitizers could be significantly enhanced by a suitable fluorescent quenching mechanism, which can be a widely applicable performance enhancing principle for QDs/NDs-SSCs. The validation of such a principle would be highly valuable for design and development of high performance QDs/NDs-SSCs.

Carbon quantum dots (CQDs) and nanodots (CNDs) are a new class of metal-free fluorophores [14-17]. Recent studies revealed that the fluorescent emission of CQDs and CNDs can be efficiently quenched by the electron accepters such as Cu^{2+}, Hg^{2+} and Fe^{3+} [18-22]. Such quenching phenomena have been successfully utilized to sensitively detect the electron accepter type of quenchers [18-22]. However, the vast majority of the reported CQDs and CNDs based fluorophores are fabricated using carbon sources that are originated from fossil fuels. It would be highly attractive to fabricate such a new class carbon materials from cheap, plentiful and renewable natural biomasses [18, 23, 24]. We recently confirmed that the fluorescent emission of graphitic CNDs obtained from grass can also be efficiently quenched by electron donors such as I^- for sensitive I^- determination in aqueous solution [24]. With graphene QDs sensitizers, an overall conversion efficiency of 0.056% was reported in an earlier study [25], and the conversion efficiency was further improved to 0.13% with CNDs sensitizers in subsequent studies (Table S1) [26-28].

In this work, N-doped CNDs synthesized from grass are chosen as the testing case to validate the proposed fluorescent quenching performance enhancement principle. The aqueous solar cells (ASCs) were assembled by a CNDs-sensitized TiO_2 photoanode and a commercial Pt counter electrode with aqueous I^-/I_3^- being used as electrolyte to serve a dual-function as the redox mediator and recombination blocker (fluorescent quencher) (denoted as CNDs-ASCs) in this work. An overall conversion efficiency of 0.529% can be achieved from a CNDs-ASC, significantly higher than the best conversion efficiency (0.13%) obtained from the CNDs-sensitized solar cells with organic solvent I^-/I_3^- electrolyte (Table S1) [25-28].

Experimental section

Synthesis of N-doped carbon nanodots (CNDs)

N-doped CNDs were synthesized by a facile hydrothermal method [18]. In a typical synthesis, 30 g fresh Monkey Grass (*Ophiopogon Japonicus*) was firstly cut into pieces and added into 60 mL of deionized water (Millipore Corp., 18 MΩ), and then the mixture was transferred into a 100 mL of Teflon lined autoclave. The hydrothermal reaction was kept at 180 °C for 6 h. After hydrothermal reaction, the obtained product was collected, respectively, by filtration (0.2 μm cellulose membrane) and centrifugation at 4,500 rpm and 14,000 rpm for 15 min to remove large-sized carbon products. The obtained nanodots suspension solution was preserved for further characterization and use. In this work, the fabricated N-doped CNDs solution has a concentration of *ca.* 35 mg/mL with a production yield of around 7.0%.

Sensitization

For more meaningful comparison, the commercially available nanocrystalline TiO_2 films with a thickness of *ca*. 10 μm (DYESOL, Australia) were used as photoanode material and firstly treated at 500 °C for 30 min prior to sensitizing with N-doped carbon nanodot solution at room temperature for 24 h. The carbon nanodot-sensitized TiO_2 films were then dried in a nitrogen stream for further use in solar cell measurements. The TiO_2 film sensitized with N-doped carbon nanodot solution was denoted as CNDs-TiO_2. The fabricated film was further treated in 100 mM I^- aqueous solution (NaI, Sigma-

Aldrich) for 30 min to form I^- modified CNDs-TiO_2 film (denoted as CNDs-TiO_2-I). After that, the CNDs-TiO_2-I film was adequately rinsed using deionized water and then dried at room temperature in a nitrogen stream for 12 h. For comparison, the CNDs-TiO_2 film was also immersed in acetonitrile containing 100 mM I^- for 30 min for further measurements. All photoanodes were preserved for further characterization and measurement in solar cells.

Characterization

Scanning electron microscope (SEM, JSM-7001F), transmission electron microscopy (TEM, Philips F20), and X-ray diffraction (XRD, Shimadzu, XRD-6000, diffractometer, equipped with a graphite monochromator) were employed for characterizing the sample structures. The UV-vis absorption of nanodot solution was measured using a Varian Cary 4500. Diffuse reflectance spectra of the photoanode films were recorded on a Varian Cary 5E ultra violet-visible-near infrared (UV-vis-NIR) spectrophotometer. FT-IR spectra of carbon nanodot sample were measured to investigate structural information and specific molecule-groups information (Perkin-Elmer 2000). Chemical compositions of the samples were analyzed by X-ray photoelectron spectroscopy (XPS, Kratos Axis ULTRA incorporating a 165 mm hemispherical electron energy analyzer). The photoluminescent (PL) spectra of carbon nanodot samples were measured on F-7000 Fluorescence Spectrophotometer (Hitachi). Carbon nanodot loading amount on nanocrystalline TiO_2 film was measured by carefully calculating the weight of TiO_2 film samples before and after sensitization.

Measurements

All investigated solar cells were fabricated with traditional sandwich type configuration by using a carbon nanodot-sensitized TiO_2 film and a platinum counter electrode deposited on FTO conducting glass (DYESOL, Australia). The organic solvent-based I^-/I_3^- electrolyte for the investigated cells was DYESOL high efficiency electrolyte (EL-HPE, the solvent is primary Acetonitrile, and iodine content is about 340 mM). The aqueous I^-/I_3^- electrolyte was prepared by mixing 0.1 M NaI and 0.01 M I_2 in deionized water. A mask with a window area of 0.15 cm^2 was applied on the TiO_2 photoanode film side to define the active area of the cells. A 500 W Xe lamp (Trusttech Co., Beijing) with an AM 1.5G filter

(Sciencetech, Canada) was used as the light source. The Light intensity was measured by a radiant power meter (Newport, 70260) coupled with a broadband probe (Newport, 70268). The photovoltaic measurements of solar cells were recorded by a scanning potentiostat (Model 362, Princeton Applied Research, US). The IPCE as a function of wavelength was measured with a QE/IPCE measurement kit (NewSpec). The Mott-Schottky relationship of the photoelectrodes were measured using a PAR 2273 electrochemical working station under a standard AM 1.5 simulated sunlight in a solution containing 0.10 M $NaNO_3$ and 0.01 M NaI. The measurements were performed in a conventional three-electrode cell (25°C), with a TiO_2/CNDs-TiO_2/CNDs-TiO_2-I photoelectrode, a saturated Ag/AgCl reference electrode and a platinum mesh counter electrode.

Results and discussion

Basic principle

As shown in Figure 1, upon the photo-excitation, an electron can be promoted from the ground-state ($\underline{C}^o$) to the excited-state ($\underline{C}^*$) of CNDs, leaving a positive charge carrier (h^+) at $\underline{C}^o$. The fate of the photo-excited electrons determines whether they could be converted to useful electricity. Without quenching, there is a high probability that the photo-excited electron would return to $\underline{C}^o$ and recombine with h^+ to generate fluorescent emission (Route I) rather than extract to the external circuit for electricity generation. It can be envisaged that the probability for a photo-excited electron to be utilized for generating electricity would be dramatically increased if Route I can be effectively inhibited. In this regard, the fluorescent quenching can be an effective means to inhibit the charge recombination. It is known that the photo-excited electrons can be quenched *via* different mechanisms. Figure 1 shows two simplistic quenching mechanisms that are directly relevance to this work. A photo-excited electron could be directly consumed by a suitable electron acceptor to achieve the fluorescent quenching (Route II) [18-21]. However, quenching in such a fashion prohibits the light-to-electricity conversion. It is known that the positive charge carriers (h^+) in the $\underline{C}^o$ of the excited CNDs possess oxidative power that can be neutralized by extracting an electron from a suitable electron donor to quench the fluorescent emission (Route III) [24]. Under such a circumstance, the probability of injecting the photo-excited

electrons into the conduction band (CB) of TiO_2 then to the external circuit would be significantly increased, which could lead to a dramatically enhanced utilization efficiency of the photo-excited electrons for electricity generation. This work will investigate the effectiveness of the fluorescent quenching *via* Route III to enhance the conversion efficiency of CNDs-sensitized solar cells. Considering majority of inorganic QDs and NDs are fluorophores, the proof of the proposed concept would have a broad implication for performance enhancement of other fluorescent QDs/NDs-sensitized solar cells.

Characterizations and optical properties

The CNDs sensitizer used in this work was synthesized by hydrothermal treatment of fresh Monkey Grass (Experimental section) [18, 24]. The transmission electron microscope (TEM) analysis indicates that the sizes of the fabricated CNDs are ranged from 2 to 6 nm (Figure 2A) [24]. Figure S1 shows the UV-vis absorption and photoluminescent (PL) emission spectra of a CNDs suspension solution. The UV-vis absorption spectrum confirms the visible absorption property, implying that the CNDs can be used as light absorbers [25-28]. The PL spectrum of the CNDs is peaked at 495 nm with an excitation wavelength of 360 nm. The XPS survey spectrum of the CNDs shown in Figure S2A confirms the presence of C, N and O. The N/C atomic ratio is determined to be 3.35%. The high resolution C 1s, N 1s and O 1s spectra of the CNDs (Figure S2B-D) reveal the presence of rich O- and N- surface functional groups, and three doped N forms (namely, pyridinic-N, pyrrolic-N and graphitic-N), consistent with the FT-IR data (Figure S3) [18, 24]. The doping of N into CNDs intruduces positively charged surfaces, facilitating interactions between I^- and graphitic carbon structures for efficient quenching [24]. In this work, the zita-potential of CNDs was measured. The obtained zita-potential of 29.8 mV confirms that the CNDs possess a positively charged surface, favorable for the I^- adsorption, which is similar to that of reported by us and others [18, 24]. The PL experiments were also performed to validate the quenching ability of I^- (Figure S4). It was found that the PL intensity of CNDs decreases with the increased I^- concentration up to 500 mM, and is very sensitive to I^- in low concentration range (*e.g.*, 0-100 mM), indicating that I^- is an effective quencher for CNDs-based fluorophores [29].

The CNDs-sensitized TiO_2 photoanodes used in this work were prepared by sensitizing an anatase dominated nanocrystalline TiO_2 film electrode (Figure 2B) with N-doped CNDs (denoted as CNDs-TiO_2). The resultant CNDs-TiO_2 photoanode exhibits a dark-brown appearance (inset in Figure 2B) with no noticeable change in TiO_2 crystal phase (Figure S5). XPS survey spectra further confirm the loading of CNDs onto TiO_2 films (Figure S6). To verify the strength of the interactions between CNDs and I^-, the CNDs-TiO_2 photoanode was immersed in an aqueous solution containing 100 mM I^- for 30 min (denoted as CNDs-TiO_2-I), then rinsed adequately with deionized water. After dried at the room temperature in a nitrogen stream, the presence of I^- is determined by XPS analysis (Figure S6 and Figure 2C). This confirms a strong interaction between CNDs and I^-, which is critically important in determining the practicality of I^- as a quencher for conversion efficiency enhancement. PL experiments were then performed to directly validate the quenching ability of the adsorbed I^-. A markedly decreased PL emission intensity observed from the CNDs-TiO_2-I electrode using aqueous solution confirms the effectiveness of the adsorbed I^- as a quencher in aqueous media (Figure 2D). For a meaningful comparison, the PL experiments of the CNDs-TiO_2 photoanode was also performed in acetonitrile containing 100 mM I^-. The fluorescence quenching ability in aqueous solution is obviously higher than that in acetonitrile (Figure 2D), suggesting the aqueous environment is favorable for photo-excited electron utilization. Similar quenching effects can also be obtained from the CNDs-TiO_2 photoanode in an assembled solar cell with aqueous and acetonitrile I^-/I_3^-electrolytes.

Solar cell performance

The performance of the CNDs-ASCs was evaluated under a standard AM 1.5 simulated sunlight (100 mW/cm^2). The curve 1# in Figure 3A shows a typical current-voltage profile of a CNDs-ASC assembled with 0.1 M I^-/0.01 M I_2 aqueous electrolyte. It reveals a short-circuit current density (J_{sc}) of 1.92 mA/cm^2, an open-circuit voltage (V_{oc}) of 498 mV and a fill factor (*FF*) of 55.3% with an overall conversion efficiency (η) of 0.529% (Table S2), which is over 4 times of the highest efficiency (0.13%) obtained to date from CNDs-sensitized solar cells with organic solvent I^-/I_3^- electrolyte (Table S1) [25-28]. The performance of a solar cell assembled using an identical CNDs-TiO_2 photoanode but

replacing the aqueous electrolyte with the acetonitrile I^-/I_3^- electrolyte containing 0.68 M I^-/0.34 M I_2 was also investigated (curve 2# in Figure 3A). It reveals a J_{sc} of 0.548 mA/cm^2, a V_{oc} of 514 mV and a *FF* of 65.3% with a η of 0.184% (Table S2), which is slightly higher than the efficiency (0.13%) reported by other groups [26-28]. Obviously, the significantly improved J_{sc} is the major factor for the higher η achieved from the aqueous electrolyte cell. This is a direct result of the effective I^- quenching in aqueous media as supported by the measured quenching efficiencies (Figure S7), where a 55% decrease in the PL emission intensity is observed from an aqueous solution containing 100 mM I^- in comparison to only 18% PL emission intensity decrease observed from the acetonitrile solution containing the same I^- concentration. The strong affinity of I^- to the CNDs in aqueous medium is advantageous for effective quenching. The higher quenching efficiency leads to a higher utilization efficiency of the photo-excited electrons for electricity generation, which is supported by the observed incident photon-to-current conversion efficiency (IPCE) spectra from the cells assembled using aqueous and acetonitrile electrolytes (Figure 3B). The superior solar cell performance in aqueous electrolyte could also be due to the hydrophilic surface of the CNDs enabling higher dispersibility in water (35 mg/mL) comparing to that in acetonitrile (15 mg/mL). The above results demonstrate that I^- quenching can play a key role to enhance the utilization efficiency of the photo-excited electrons for electricity generation. It is known that for a given quencher, the quenching performance can be highly dependent on the quencher concentration. The effect of I^- concentration on light conversion efficiency of the CNDs-ASCs was therefore investigated. The results indicate that J_{sc} dramatically decreased with a low I^- concentration of 0.05 M, leading to a lower overall efficiency of 0.237% (Figure S8). A high I^- concentration of 0.5 M enables a high J_{sc} but low V_{oc} and *FF*, resulting a decrease in overall conversion efficiency to 0.506% (Figure S8). The decreased V_{oc}, and *FF* at high I^- concentration might be due to the formation of large number of I-induced trapping energy states [30].

The above results demonstrate the effectiveness of the proposed fluorescent quenching performance enhancement principle. We have assumed that I^- quenching is achieved *via* Route III (Figure 1), where

upon CNDs absorbing a photon, an electron is promoted to $\underline{C}^*$ of CNDs ($\underline{C}^*$[28]), creating a positive charge carrier at $\underline{C}^o$ ($\underline{C}^o\{h^+\}$:

$$CNDs \xrightarrow{h\nu} \underline{C}^*\{e^-\} + \underline{C}^o\{h^+\} \qquad (1)$$

then, I^- as a quencher donates an electron to neutralize $\underline{C}^o\{h^+\}$, leading to the production of I_3^-:

$$3I^- + \underline{C}^o\{2h^+\} \longrightarrow \underline{C}^o\{0\} + I_3^- \qquad (2)$$

That is, if the above reactions proceeded, the produced I_3^- should be detectable when a CNDs suspension solution containing I^- is illuminated. Figure 4 shows the UV-vis absorption spectra of CNDs suspension solutions with 1.0 mM I^- or in absence of I^-, under different illumination times with AM 1.5 simulated sunlight (100 mW/cm^2). To eliminate the influence of O_2 on I^- oxidation, all solutions were purged with N_2 during experiments. In absence of I^-, with or without illumination, only one absorption band centered at 275 nm can be observed, consistent with the reported CNDs spectra [18, 24, 29]. In absence of CNDs, the UV-vis absorption spectrum obtained from a 1.0 mM I^- aqueous solution displays a typical absorption spectrum of I^- with a single absorption band centered at 226 nm (Figure S9) [31]. The UV-vis absorption spectra obtained from the illuminated CNDs suspension solution containing 1.0 mM I^- show two distinctive I_3^- absorption bands centered at 288 and 350 nm [31], respectively (Figure 4), which differs obviously from that observed from CNDs suspension or I^- solution in absence of CNDs. The intensity of these I_3^- absorption peaks increases with the illumination time (the inset in Figure 4), indicating the increased production of I_3^-. Such experimental results confirm that I^- quenching does occur and is *via* Route III in accordance with Equation 2. Although an efficient conversion of I^- into I_3^- at CNDs is confirmed, to enable I^- serves its role as a redox mediator, the produced I_3^- must be regenerated at the Pt counter electrode. In fact, the energy of $\underline{C}^*$[28] also needs to match the conduction band (CB) energy of TiO_2 to enable the electron injection.

Band structure

The energy band structures of the CNDs-ASC were therefore determined. In comparison to TiO_2, the CNDs-TiO_2 and CNDs-TiO_2-I films exhibit superior visible light absorption capability (Figure S10A). An almost identical bandgap of 1.59 eV is determined for both CNDs-TiO_2 and CNDs-TiO_2-I (Figure

S10B), suggesting the adsorbed I^- has insignificant influence on the energy band structure of CNDs. The bandgap for TiO_2 is determined to be 3.18 eV (Figure S10B). Figure S11 shows the Mott-Schottky plots of CNDs-TiO_2 and TiO_2 electrodes under a standard AM 1.5 simulated sunlight. The determined flat-band potentials for CNDs-TiO_2 and TiO_2 electrodes are -496 and -328 mV (*vs* Ag/AgCl), respectively. The calculated energy band structures of TiO_2 and CNDs based on these measured bandgaps and flat-band potentials are schematically illustrated in Figure 5. The energy of $\underline{C}$*[28] (-4.14 eV) is 0.17 eV more positive than the CB energy of TiO_2 (-4.31 eV), confirming that photo-excited electrons ($\underline{C}$*[28]) can be simultaneously injected into the CB of TiO_2. The $\underline{C}^o\{h^+\}$ possesses a oxidation power of -5.73 eV, more than sufficient to oxidize I^- into I_3^- ($E^o\{I^-/I_3^-\}$ = -4.97 eV) in the quenching process. The theoretical cell potential difference of the CNDs-ASC is 0.66 eV, which can readily reduce I_3^- into I^-, realizing I^- regeneration at Pt counter electrode. That is, I^- serves a role of charge recombination blocker (fluorescent quencher) in the photoelectron injection process and also acts as a redox mediator in the electrochemical process.

Although the quenching approach presented in this work has demonstrated to markedly improve the conversion efficiency of CNDs-ASC to a level that is over 4 times of the best performed CNDs-sensitized solar cells reported to date, the achieved efficiency of 0.529% is still low compared to other types of QDs/NDs-SSCs [1-6]. This could be due to the low quantum yield of photo-excited electrons generation at the illuminated N-doped CNDs for photovoltaic application [32]. It is envisaged that the quenching performance enhancement principle could be more effective for QDs or NDs sensitizers possessing higher fluorescent quantum yields.

Conclusions

In summary, we have proposed and experimentally validated a fluorescent quenching principle capable of markedly enhancing the utilization efficiency of the photo-excited electrons generated by the fluorescent CNDs sensitizers to improve the conversion efficiency of CNDs-sensitized aqueous solar cells, which could be a widely applicable performance enhancement principle to improve the performance of other fluorescent QDs/NDs-sensitizers solar cells.

Acknowledgements

This work was financially supported by Australian Research Council (ARC) Discovery Project and the Natural Science Foundation of China (Grant Nos. 51372248, 51432009).

Appendix A. Supporting information

Supplementary data associated with this work can be found in the online version at http://dx.doi.org/

References

[1] H. McDaniel, N. Fuke, N.S. Makarov, J.M. Pietryga, V.I. Klimov, Nat. Commun. 4 (2013) 1-10.
[2] A.H. Ip, S.M. Thon, S. Hoogland, O. Voznyy, D. Zhitomirsky, R. Debnath, L. Levina, L.R. Rollny, G.H. Carey, A. Fischer, K.W. Kemp, I.J. Kramer, Z. Ning, A.J. Labelle, K.W. Chou, A. Amassian, E.H. Sargent, Nat. Nanotechnol. 7 (2012) 577-582.
[3] E.H. Sargent, Nat. Photonics 6 (2012) 133-135.
[4] L. Li, X. Yang, J. Gao, H. Tian, J. Zhao, A. Hagfeldt, L. Sun, J. Am. Chem. Soc. 133 (2011) 8458-8460.
[5] P.K. Santra, P.V. Kamat, J. Am. Chem. Soc. 134 (2012) 2508-2511.
[6] H.-S. Rao, W.-Q. Wu, Y. Liu, Y.-F. Xu, B.-X. Chen, H.-Y. Chen, D.-B. Kuang, C.-Y. Su, Nano Energy 8 (2014) 1-8.
[7] B. O'Regan, M. Graetzel, Nature 353 (1991) 737-740.
[8] M. Liu, M.B. Johnston, H.J. Snaith, Nature 501 (2013) 395-398.
[9] S.D. Stranks, G.E. Eperon, G. Grancini, C. Menelaou, M.J.P. Alcocer, T. Leijtens, L.M. Herz, A. Petrozza, H.J. Snaith, Science 342 (2013) 341-344.
[10] J. Burschka, N. Pellet, S.-J. Moon, R. Humphry-Baker, P. Gao, M.K. Nazeeruddin, M. Graetzel, Nature 499 (2013) 316-319.
[11] Y. Chen, J. Vela, H. Htoon, J.L. Casson, D.J. Werder, D.A. Bussian, V.I. Klimov, J.A. Hollingsworth, J. Am. Chem. Soc. 130 (2008) 5026-5027.
[12] Y. Jin, X. Gao, Nat. Nanotechnol. 4 (2009) 571-576.
[13] M.-K. So, A.M. Loening, S.S. Gambhir, J. Rao, Nat. Protoc. 1 (2006) 1160-1164.
[14] Y.-P. Sun, B. Zhou, Y. Lin, W. Wang, K.A.S. Fernando, P. Pathak, M.J. Meziani, B.A. Harruff, X. Wang, H. Wang, P.G. Luo, H. Yang, M.E. Kose, B. Chen, L.M. Veca, S.-Y. Xie, J. Am. Chem. Soc. 128 (2006) 7756-7757.
[15] S.N. Baker, G.A. Baker, Angew. Chem., Int. Ed. 49 (2010) 6726-6744.
[16] S. Qu, X. Wang, Q. Lu, X. Liu, L. Wang, Angew. Chem., Int. Ed. 51 (2012) 12215-12218.
[17] V. Gupta, N. Chaudhary, R. Srivastava, G.D. Sharma, R. Bhardwaj, S. Chand, J. Am. Chem. Soc. 133 (2011) 9960-9963.
[18] S. Liu, J. Tian, L. Wang, Y. Zhang, X. Qin, Y. Luo, A.M. Asiri, A.O. Al-Youbi, X. Sun, Adv. Mater. 24 (2012) 2037-2041.
[19] Y. Dong, R. Wang, G. Li, C. Chen, Y. Chi, G. Chen, Anal. Chem. 84 (2012) 6220-6224.
[20] R. Kramer, Angew. Chem., Int. Ed. 37 (1998) 772-773.
[21] L. Zhou, Y. Lin, Z. Huang, J. Ren, X. Qu, Chem. Commun. 48 (2012) 1147-1149.
[22] S. Zhu, Q. Meng, L. Wang, J. Zhang, Y. Song, H. Jin, K. Zhang, H. Sun, H. Wang, B. Yang, Angew. Chem., Int. Ed. 52 (2013) 3953-3957.
[23] H. Zhang, Y. Wang, D. Wang, Y. Li, X. Liu, P. Liu, H. Yang, T. An, Z. Tang, H. Zhao, Small 10 (2014) 3371-3378.
[24] H. Zhang, Y. Li, X. Liu, P. Liu, Y. Wang, T. An, H. Yang, D. Jing, H. Zhao, Environ. Sci. Technol. Lett. 1 (2014) 87-91.

[25] X. Yan, X. Cui, B. Li, L.-s. Li, Nano Lett. 10 (2010) 1869-1873.
[26] P. Mirtchev, E.J. Henderson, N. Soheilnia, C.M. Yip, G.A. Ozin, J. Mater. Chem. 22 (2012) 1265-1269.
[27] C. Wang, X. Wu, X. Li, W. Wang, L. Wang, M. Gu, Q. Li, J. Mater. Chem. 22 (2012) 15522-15525.
[28] Y.-Q. Zhang, D.-K. Ma, Y.-G. Zhang, W. Chen, S.-M. Huang, Nano Energy 2 (2013) 545-552.
[29] H. Li, Z. Kang, Y. Liu, S.-T. Lee, J. Mater. Chem. 47 (2012) 24230-24253.
[30] S. Tojo, T. Tachikawa, M. Fujitsuka, T. Majima, J. Phys. Chem. C 112 (2008) 14948-14954.
[31] J.J. Custer, S. Natelson, Anal. Chem. 21 (1949) 1005-1009.
[32] F. Deschler, M. Price, S. Pathak, L. Klintberg, D.D. Jarausch, R. Higler, S. Huettner, T. Leijtens, S.D. Stranks, H.J. Snaith, M. Atature, R.T. Phillips, R.H. Friend, J. Phys. Chem. Lett. 5 (2014) 1421-1426.

`

Figure Captions

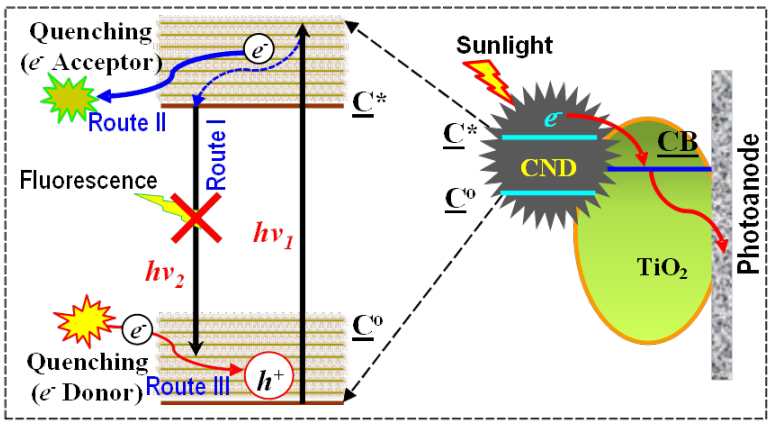

Figure 1 Schematic illustration of the photo-excited electron quenched by an electron acceptor (Route II) and donor (Route III).

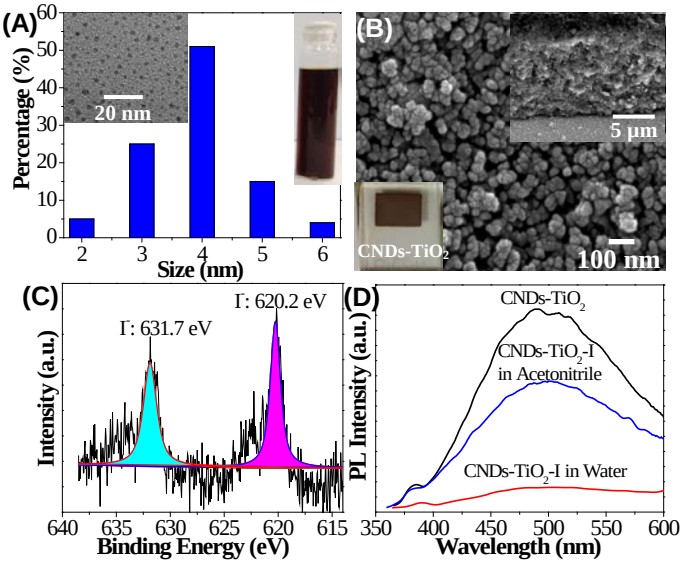

Figure 2 (A) Size distribution of CNDs with the insets of TEM image and the photo of CNDs sample. (B) Surface SEM image of nanocrystalline TiO_2 film, the top inset: cross-sectional SEM image, the bottom inset: photo of CNDs-TiO_2 photoanode. (C) High resolution I 3d XPS spectra of CNDs-TiO_2 film with adsorbed I^-. (D) PL spectra of CNDs-TiO_2 and CNDs-TiO_2-I films in water and acetonitrile with a 350 nm excitation wavelength.

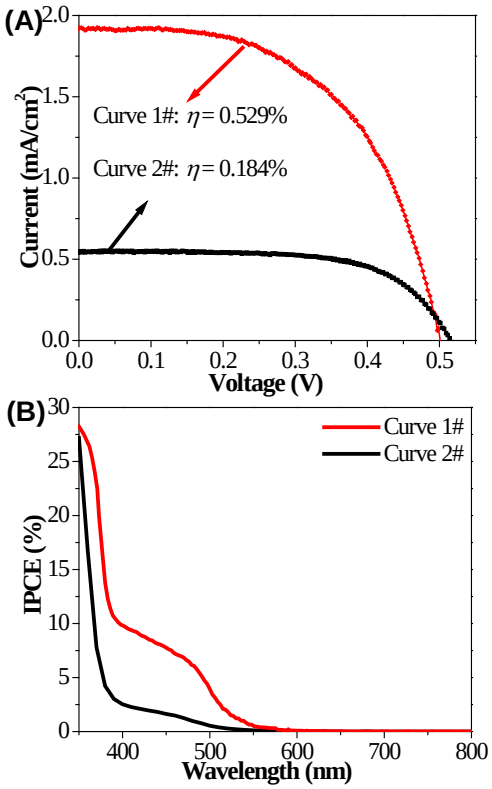

Figure 3 (A) Current–voltage characteristics of solar cells assembled with CNDs-TiO_2 photoanodes using aqueous (Curve 1#) and acetonitrile (Curve 2#) I^-/I_3^- electrolytes. (B) IPCE spectra of solar cells assembled with CNDs-TiO_2 photoanodes using aqueous (Curve 1#) and acetonitrile (Curve 2#) I^-/I_3^- electrolytes.

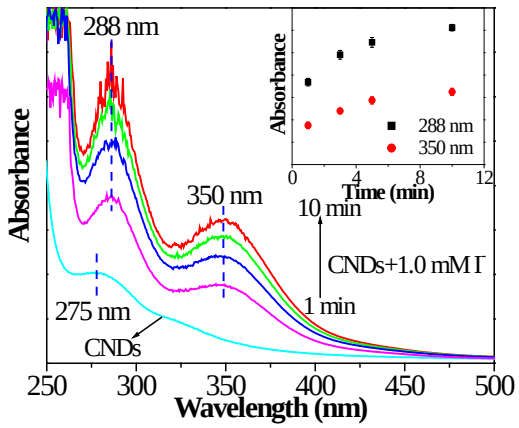

Figure 4 UV-vis absorption spectra of CNDs suspension solution containing 1.0 mM I^- under the illumination of AM 1.5 simulated sunlight, the inset is the plots of the absorption peak intensities at 288 nm and 350 nm versus illumination time.

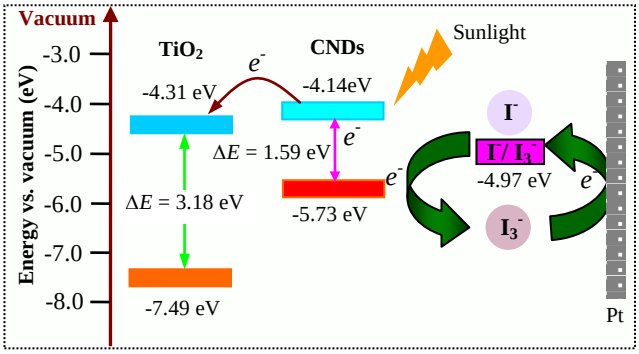

Figure 5 Schematic illumination of energy band structures of CNDs-ASC.